



Enhanced chlorine enrichment via electron-deficient centers of Co(III) for efficient electrochlorination and ammonia removal

Lei Tian ^{a,b,1}, Xing-Yuan Xia ^{a,1}, Li-Juan Zhou ^a, Ling-Ling Zheng ^a, Qiu-Ju Xing ^a, Long-Shuai Zhang ^a, Jian-Ping Zou ^{a,*}, Zhao-Qing Liu ^{b,*}

^a National-Local Joint Engineering Research Center of Heavy Metals Pollutants Control and Resource Utilization, Nanchang Hangkong University, Nanchang 330063, PR China

^b School of Chemistry and Chemical Engineering/Institute of Clean Energy and Materials/Guangzhou Key Laboratory for Clean Energy and Materials/Key Laboratory for Water Quality and Conservation of the Pearl River Delta, Ministry of Education, Guangzhou University, Guangzhou 510006, PR China

ARTICLE INFO

Keywords:

Ammonia
Chlorine evolution reaction
Electrocatalytic system
Electron-deficient centers
Nitrogen

ABSTRACT

Subject to the sluggish enrichment kinetics of Cl^- at anodic active sites, the chlorine evolution reaction (CER) activity and selectivity of current anodes are dissatisfaction for the treatment of ammonia-containing wastewater. In this study, antimony and stannum with strong electronegativity are synchronously introduced into cobaltosic oxide ($\text{Sb}_2\text{O}_5\text{-Co}_3\text{O}_4/\text{Sn}$) to induce the construction of Co(III) sites with robust electron-deficient centers. The formation of such electron-deficient centers of Co(III) strengthens the enrichment of Cl^- and broadened the potential difference of chlorine/oxygen evolution, thereby promoting the CER activity and selectivity at low Cl^- concentration. 50.0 mg/L of ammonia-nitrogen can be mineralized into nitrogen within 90 min in the EC system assembled with $\text{Sb}_2\text{O}_5\text{-Co}_3\text{O}_4/\text{Sn}$ anode, which is superior to that of the commercial dimensionally stable anode. Finally, the system shows exceptional feasibility of practical ammonia-containing wastewater purification. This study opens novel avenues to design anodes for highly selective CER and efficient treatment of ammonia-contaminated effluents.

1. Introduction

Ammonia ($\text{NH}_4^+/\text{NH}_3$) is widely used in chemical plants and electronic industries, resulting in the generation of a large amount of ammonia-containing wastewater. A series of ecological problems can be induced by the discharge of ammonia-containing wastewater [1–4]. Nowadays, the emission limitation standard of ammonia is becoming more and more strict [5,6]. Therefore, it is significant to develop efficient strategies for the treatment of ammonia-containing wastewater.

At present, breakpoint chlorination is the most common strategy for the treatment of ammonia-containing wastewater due to its highly efficient and selective mineralization of ammonia into nitrogen (N_2) (Eqs. 1–2) [7–10]. However, subject to the high cost and hard storage/transportation of chlorine, the application of breakpoint chlorination has been greatly restrained. For the substitution of conventional breakpoint chlorination, in-situ chlorine evolution reaction (CER) in the electrocatalytic system (EC) is widely developed [11–13]. Dimensionally stable anodes (DSAs), based on ruthenium (Ru) and iridium (Ir),

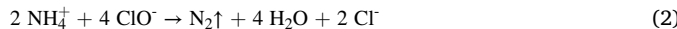
have been predominantly employed as the CER catalysts for the elimination of ammonia pollution [14–16]. Nevertheless, except for the scarcity and high price of precious metals, the CER selectivity of the DSAs during the ammonoxidation process is relatively inferior (below 70%). It is because that DSAs are also highly active for the oxygen evolution reaction (OER), suggesting that the OER and CER are intimately coupled [17,18]. More importantly, due to the low amount of chloride ions (Cl^-) required during the ammonoxidation process, the slow diffusion of Cl^- further weakens the CER selectivity of DSAs. As a result, the removal performance of ammonia in the EC system assembled with DSAs is low-efficient. Though various advanced electrocatalysts have been pursued, such as the atomically dispersed $\text{Ru}_1\text{TiO}_2/\text{Ti}$ and Pt_1/CNT , to promote the anodic CER selectivity (over 90% at low concentration of Cl^-) [19–21], the harsh synthesis process and high-cost limit their industrial application. Therefore, it is urgent to develop novel anodes with low cost, high activity, and selectivity of CER performance by using earth-abundant elements to achieve the efficient treatment of ammonia-containing wastewater.

* Corresponding authors.

E-mail addresses: jzp_112@126.com (J.-P. Zou), lzqgzu@gzhu.edu.cn (Z.-Q. Liu).

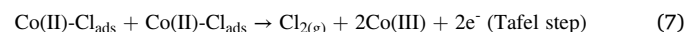
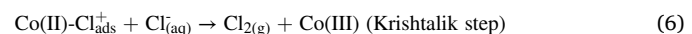
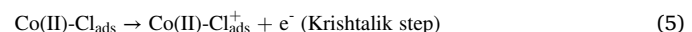
¹ These authors contributed equally to this work.





Benefiting from the outstanding Co(II)/Co(III) cycle and high redox potential of Co(III) ($E^0 = 1.81$ V), cobaltic oxides (Co_3O_4) have attracted much attention as the CER electrocatalysts for the purification of ammonia-containing wastewater [22,23]. As demonstrated in Eqs. 3–7, the formation of Cl_2 at the Co_3O_4 anode is derived from the enrichment of Cl^- at the structural Co(III), which plays a governing role in the CER activity and selectivity. Subsequently, Cl^- is activated by Co(III) into the adsorbed chlorine radical (Cl_{ads} or Cl^{\bullet}) and is further self-quenched to form Cl_2 [20,24,25]. However, due to the sluggish enrichment kinetics of Cl^- at the structural Co(III) (Volmer step), the CER activity and selectivity of current Co_3O_4 anodes are barely satisfactory. The efficient enrichment of Cl^- at the structural Co(III) sites plays a decisive role in enhancing the CER activity and selectivity of the Co_3O_4 anode. It is well-known that the outer electronic orbitals of Cl^- contain a large number of lone pair electrons, which have strong interactions with the vacancies at the outer orbitals of transition metals [26]. Therefore, if the structural Co(III) sites with strong electron-deficient centers could be constructed on the Co_3O_4 anode to strengthen the enrichment of Cl^- , the CER activity and selectivity of Co_3O_4 would be effectively improved,

thereby promoting the mineralization of ammonia in the EC system.



To verify the above hypothesis, stannum (Sn, electronegativity: 1.96) and antimony (Sb, 2.05), which are more electronegative than Co (1.88), are introduced into the Co_3O_4 anode by a one-pot solvothermal method as a heterojunction or dopant, which is the general strategy to regulate the electronic structure of active sites. Theoretically speaking, the electrons of Co(III) are induced to migrate to Sn and Sb, resulting in the formation of Co(III) sites with strong electron-deficient centers. The combination form (heterojunction or doping) between Sb/Sn and Co_3O_4 is elaborately analyzed through structural characterizations. Besides, the CER activity and ammonia removal performance of raw Co_3O_4 , modified Co_3O_4 , and commercial DSAs are compared by batch experiments and electrochemical characterizations. Moreover, X-ray photoelectron spectroscopy (XPS) and density functional theory (DFT) are

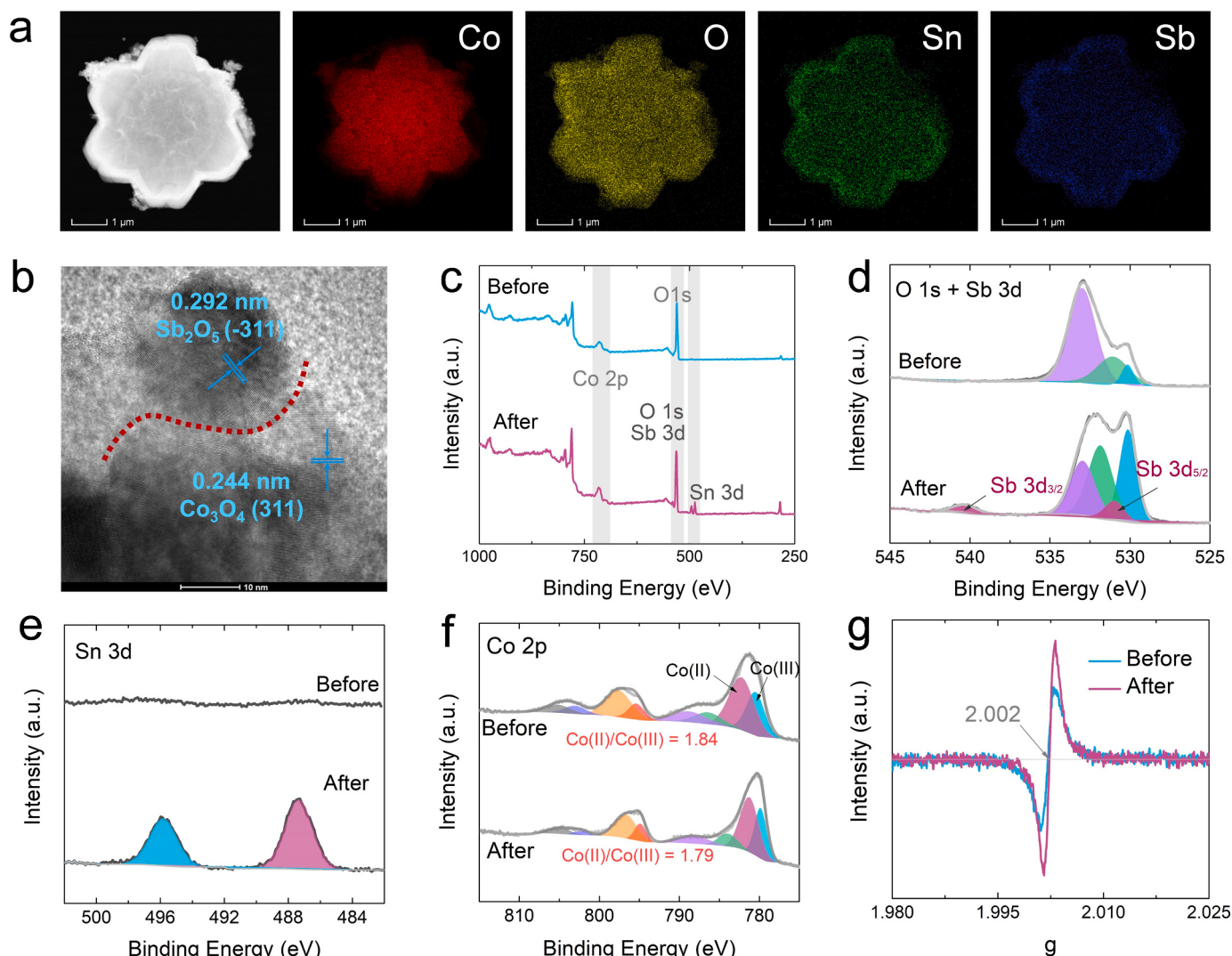


Fig. 1. (a) EDX mapping images and (b) HRTEM image of Co_3O_4 modified by Sn and Sb; XPS spectra of (c) survey, (d) O 1 s + Sb 3d, (e) Sn 3d and (f) Co 2p of Co_3O_4 before and after modification with Sn and Sb; (g) EPR patterns of Co_3O_4 before and after modification with Sn and Sb.

used to further investigate the mechanisms of the electron-deficient centers' formation and the CER enhancement after the introduction of Sn and Sb. Finally, the EC system with the modified Co_3O_4 anode is used to treat the practical pickle wastewater (NH_4^+ -N: 135 mg/L) and investigate its feasibility for the treatment of ammonia-containing wastewater. This work provides new insights for efficient and low-cost design to enhance CER performance and ammonia remediation.

2. Materials and methods

2.1. Chemicals and materials

All chemicals were commercially obtained and used without further purification. Detailed information is provided in Text S1 in the Supporting Information (SI).

2.2. Synthesis of anode

The anode modified by Sn and Sb was prepared by a hydrothermal-calcination method. $\text{Co}(\text{NO}_3)_2 \cdot 6 \text{H}_2\text{O}$ (0.582 g), SbCl_3 , and $\text{SnCl}_4 \cdot 5 \text{H}_2\text{O}$ with a certain molar ratio were added sequentially to a mixture of ethylene glycol (10 mL) and deionized water (30 mL). Then, urea (0.5 g), cetyltrimethylammonium bromide (0.05 g), and ammonium fluoride (1.455 g) were added and stirred for 30 min to form a homogeneous and transparent solution. The solution was transferred to a 100 mL Teflon liner and a piece of fluorine-doped tin oxide (FTO, 1.5 cm \times 4.0 cm) substrate with the conductive side up was dipped into the above solution. The autoclave was kept at 120 °C for 12 h. The electrodes were then calcined in a muffle furnace under the air atmosphere at 350 °C for 2 h, and at 550 °C for another 2 h. The heating rate was 1 °C/min. Except for that only SbCl_3 or $\text{SnCl}_4 \cdot 5 \text{H}_2\text{O}$ was added, the synthesis steps of the anode modified by Sb or Sn individually were the same as above.

2.3. Degradation performance evaluation

The concentrations of all nitrogen-containing species were calculated in terms of nitrogen atoms (N) in this work. About 100 mL of ammonia solution (50 mg/L, NH_4^+ -N) was added to an undivided cylindrical glass electrolytic cell (A schematic diagram was provided in Fig. S1). The different anodes and the Pt cathode were fixed at a gap of 1 cm in the reactor and connected to a potentiostat (CHI 660E electrochemical workstation (Shanghai, Chenhua, China)). Ag/AgCl was used as the reference electrode. Before the reaction, 50 mM NaCl was added as the electrolyte to improve mass transfer and provide a source of chlorine. The immersed area of the electrode was 4.5 cm². During the reaction process, the samples were taken with syringes at designated time intervals and immediately filtered through 0.45 μm polytetrafluoroethylene (PTFE) membranes. All experiments were conducted three times.

2.4. Analytical methods

Ammonia ($\text{NH}_3/\text{NH}_4^+$) was measured at 420 nm using Nessler's reagent method in a spectrophotometer (UV-9000S, Metash Instruments Ltd, China) [27]. The total nitrogen (TN) concentration was determined by the alkaline potassium persulfate method in an anaerobic digester (DRB200, HACH Co, USA) [27]. Nitrate (NO_3^-) and nitrite (NO_2^-) concentrations were measured using an ion chromatography system (Dionex-120, Dionex Inc, USA). Free chlorine (Cl_2 , HClO , ClO^-) concentration was determined by N,N-diethyl-1,4-phenylenediamine sulfate (DPD) spectrophotometry and the CER selectivity was measured according to the previous literature (Text S2) [21,28]. Nitrobenzene (NB), tert-butanol (TBA), and carbamazepine (CBZ) were used as the quenchers of free radicals to qualitatively analyze the effect of $\cdot\text{OH}$, $\text{Cl}\cdot$, $\text{ClO}\cdot$, and Cl_2^- on the ammonia removal in the EC system. The metal ion concentrations in the solution were detected by an

inductively coupled plasma optical emission spectrometer (ICP-OES 7400, Thermo Fisher, USA). Resonance (EPR) spectra were measured by a Bruker A300 spectrometer (Germany). DFT on differential charge distribution and adsorption energy (E_{ads}) were conducted to reveal the electronic structure of the anode and the enrichment kinetics between Cl^- and the anode. Details of theoretical calculations were presented in Text S3. The calculation method of the energy consumption was exhibited in Text S4.

3. Results and discussion

3.1. Structure of Sn and Sb co-modified Co_3O_4

As shown in Fig. S2, the Co_3O_4 before and after modification demonstrate typical 3D hexagonal flower shapes. EDX mapping results reveal that there are four elements, including Co, O, Sb, and Sn, uniformly distributed throughout the modified Co_3O_4 (Fig. 1a). Besides, as exhibited in Fig. S3 in the SI, four typical diffraction peaks in XRD spectra are observed at 20 of 31.27°, 36.85°, 59.36°, and 65.24° for both Co_3O_4 and modified Co_3O_4 , which are indexed to (2 2 0), (3 1 1), (5 1 1) and (4 4 0) planes of Co_3O_4 (JCPDS#42-1467) crystal structure, respectively [29–31]. Moreover, Raman spectra (Fig. S4) demonstrate that five modes ($E_g + A_1g + 3 F_2g$) of Co_3O_4 before and after modification are attributed to the spinel structure of Co_3O_4 [32,33]. It's worth noting that a peak shift of $F_2^{(3)}g$ and A_1g is observed, indicating a slight change in the electronic configuration of Co after the introduction of Sb and Sn. The above results verify the successful introduction of Sb and Sn into Co_3O_4 and it does not change the crystalline structure of Co_3O_4 .

To further analyze the structure of the modified Co_3O_4 , high-resolution transmission electron microscopy (HRTEM) is carried out. As exhibited in Fig. 1b, there is a heterojunction between the (-3 1 1) crystal plane of Sb_2O_5 and the (3 1 1) crystal plane of Co_3O_4 in the modified Co_3O_4 , demonstrating Sb is compounded with Co_3O_4 as a form of Sb_2O_5 (Fig. 1f). As a comparison, though the amount of Sn is much larger than that of Sb (Table S1), the crystal plane of SnO_2 is not observed in the HRTEM image, inferring the possible doping of Sn into Co_3O_4 . XPS is used to figure out the doping sites of Sn. As illustrated in Figs. 1c–1e, several strong peaks assigned to Co 2p, Sb 3d, O 1s, and Sn 3d are observed in the XPS spectra of the modified Co_3O_4 . The peak at 530 eV in O 1s is attributable to lattice oxygen and its intensity increases significantly after the introduction of Sn and Sb (Fig. 1d), resulting from the possible formation of heterogeneous oxides. The peaks at 540.3 and 531.0 eV in Sb 3d spectra and the peaks at 495.8 and 487.5 eV in Sn 3d spectra are assigned to the characteristic peaks of Sb (V)-O and Sn(IV)-O bonds, respectively (Figs. 1d and 1e) [34,35]. Remarkably, by comparing the contents of Co(II) and Co(III) of Co_3O_4 before and after modification in Co 2p_{3/2} XPS spectra, it is found that the ratio of Co(II)/Co(III) decreases from 1.84 to 1.79 after the simultaneous introduction of Sn and Sb (Fig. 1f). The same phenomenon is also observed when Sn is solely introduced into Co_3O_4 (Fig. S5). Since the ratio of Co(II)/Co(III) maintains constant after the individual introduction of Sb, the decrease of the ratio of Co(II)/Co(III) after the simultaneous introduction of Sn and Sb should be attributed to the occupation of Co(II) sites in tetrahedron by Sn [36]. In addition, electron paramagnetic resonance (EPR) is applied to explore the doping sites of Sn because the occupation of Co(II) sites in tetrahedrons by Sn(IV) could induce the formation of oxygen vacancies. As shown in Fig. 1g and S6, stronger EPR signals are observed after the modification of individual Sn or both Sb and Sn, and there are no significant differences between pristine Co_3O_4 and the Co_3O_4 modified by Sb, indicating the formation of oxygen vacancies with the introduction of Sn. This result further verifies the occupation of Co(II) sites in tetrahedrons by Sn(IV). Based on the above results, it can be summarized that the combination forms of Sb and Sn with Co_3O_4 are different, where Sb_2O_5 compounds with Co_3O_4 as a heterojunction while Sn dopes at Co(II) sites in the tetrahedron of Co_3O_4 . The structure diagram of the modified Co_3O_4 is exhibited in

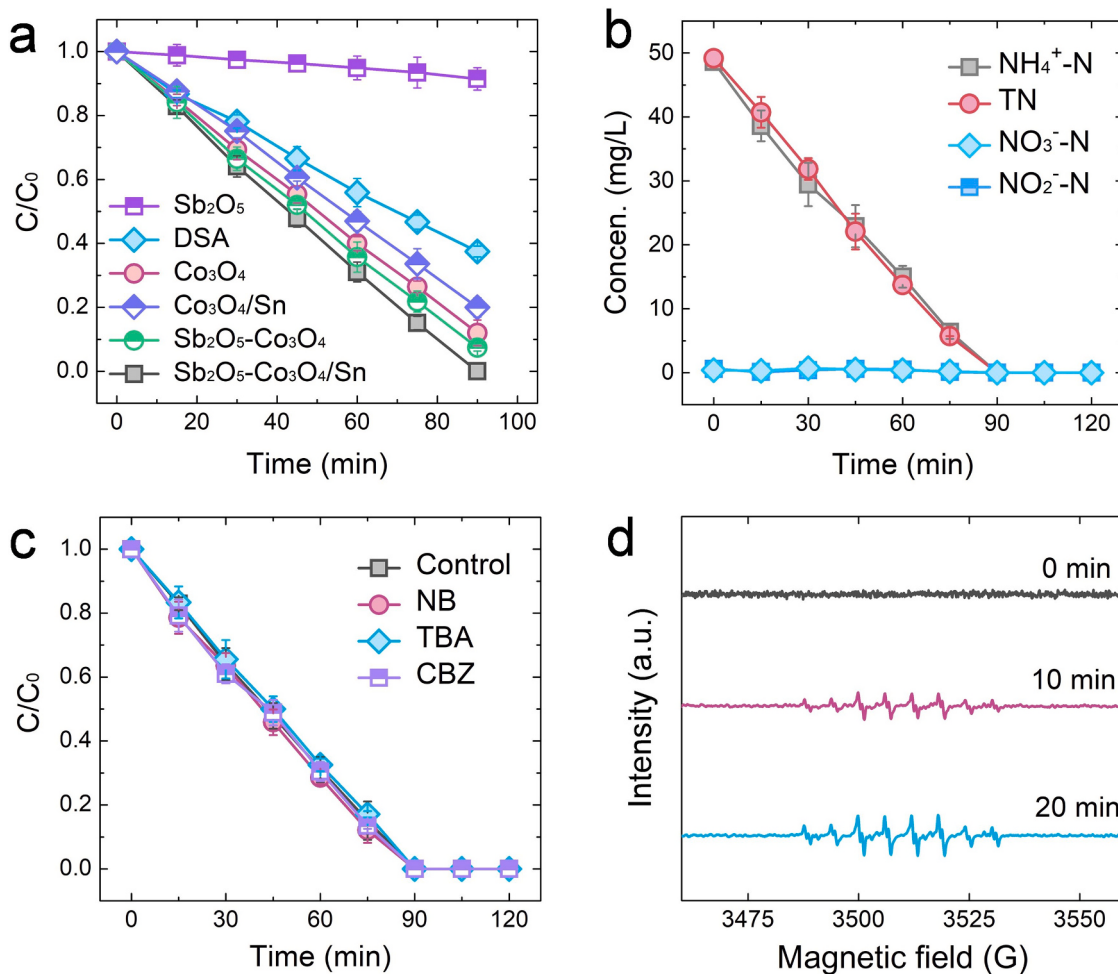


Fig. 2. (a) Ammonia removal performance in the EC system with different anodes; (b) Concentration change of different nitrogen species in the EC system with Sb₂O₅-Co₃O₄/Sn anode; (c) Ammonia removal in the EC systems with different scavengers; (d) EPR spectra in the EC system. Conditions: [NH₄⁺-N] = 50 mg/L, [NaCl] = 50 mM, pH = 6, [scavengers] = 10 mM, constant current = 20 mA.

Fig. S7. During the following experiment, the modified Co₃O₄ is named Sb₂O₅-Co₃O₄/Sn.

3.2. Removal performance of ammonia

3.2.1. Influence factors

The impacts of the additive amount of Sn and Sb source, the electrolyte concentration, and the initial pH value on the ammonia removal process in the EC system are of particular interest. As illustrated in Figs. S8 and S9, with the increase of the molar ratio of Sn and Sb sources to Co source from 1% to 9%, the ratio of ammonia removal displays an increase followed by a decrease. When the additive amount of Sn and Sb sources are 5% and 5% respectively, the optimum removal rate of ammonia is 0.025 min⁻¹. Besides, as exhibited in Fig. S10, the removal performance of ammonia increases with the increase of NaCl electrolyte concentrations from 0 to 50 mM. Due to the excellent CER performance of the Sb₂O₅-Co₃O₄/Sn anode, the increase of Cl⁻ concentration can effectively promote the formation of free chlorines (Cl₂, HClO, ClO⁻), further improving the ammonia removal efficiency [37–39]. However, when the concentration of NaCl electrolyte reaches 70 mM, the enhanced removal performance of ammonia is negligible. This phenomenon is mainly related to the quenching of free chlorines into perchlorates (ClO₄⁻) caused by excess Cl⁻, which has a low activity for ammonia oxidation [40]. In addition, the ammonia removal performance has not been significantly changed with the variation of initial pH (3–11) (Fig. S11), indicating the excellent pH application range of the EC

system. Based on the above results, all subsequent removal experiments are conducted with 5% Sb and 5% Sn sources in anode preparation, a NaCl concentration of 50 mM.

To further investigate the superiority of the Sb₂O₅-Co₃O₄/Sn electrode, the ammonia removal performance in the EC systems with different anodes is compared. As illustrated in Fig. 2a, and S12, when Co₃O₄ and the commercial DSAs are used as the anodes, the ammonia removal is 89% and 62% with a rate of 0.021 min⁻¹ and 0.012 min⁻¹, respectively. As a comparison, after the introduction of Sb and Sn alone, about 92% and 79% of ammonia are removed in the EC system with Sb₂O₅/Co₃O₄ and Co₃O₄/Sn anodes, respectively. The individual introduction of Sn into Co₃O₄ causes the inhibition of ammonia removal attributed to the substitution of Co(II) in Co₃O₄ by Sn, slightly restraining the cycle of Co(II)/Co(III) and the CER performance of the anode. Remarkably, nearly 100% of ammonia is eliminated at a rate of 0.025 min⁻¹ in the EC system with Sb₂O₅-Co₃O₄/Sn anode. The simultaneous introduction of Sb and Sn into Co₃O₄ greatly promotes the efficient removal of ammonia, indicating that there is a synergistic effect between Sb and Sn to enhance the CER activity of Co₃O₄, thereby promoting the removal of ammonia. In addition, as demonstrated in Fig. 2b and S13, the concentration of TN decreases synchronously with the reduction of ammonia concentration and no undesired products (such as NO₂, NO₃, and chloramines) generate after the reaction, manifesting that ammonia can be efficiently and selectively mineralized into N₂ in the EC system. These results indicate that Sb₂O₅-Co₃O₄/Sn anode demonstrates more outstanding performance for ammonia removal than

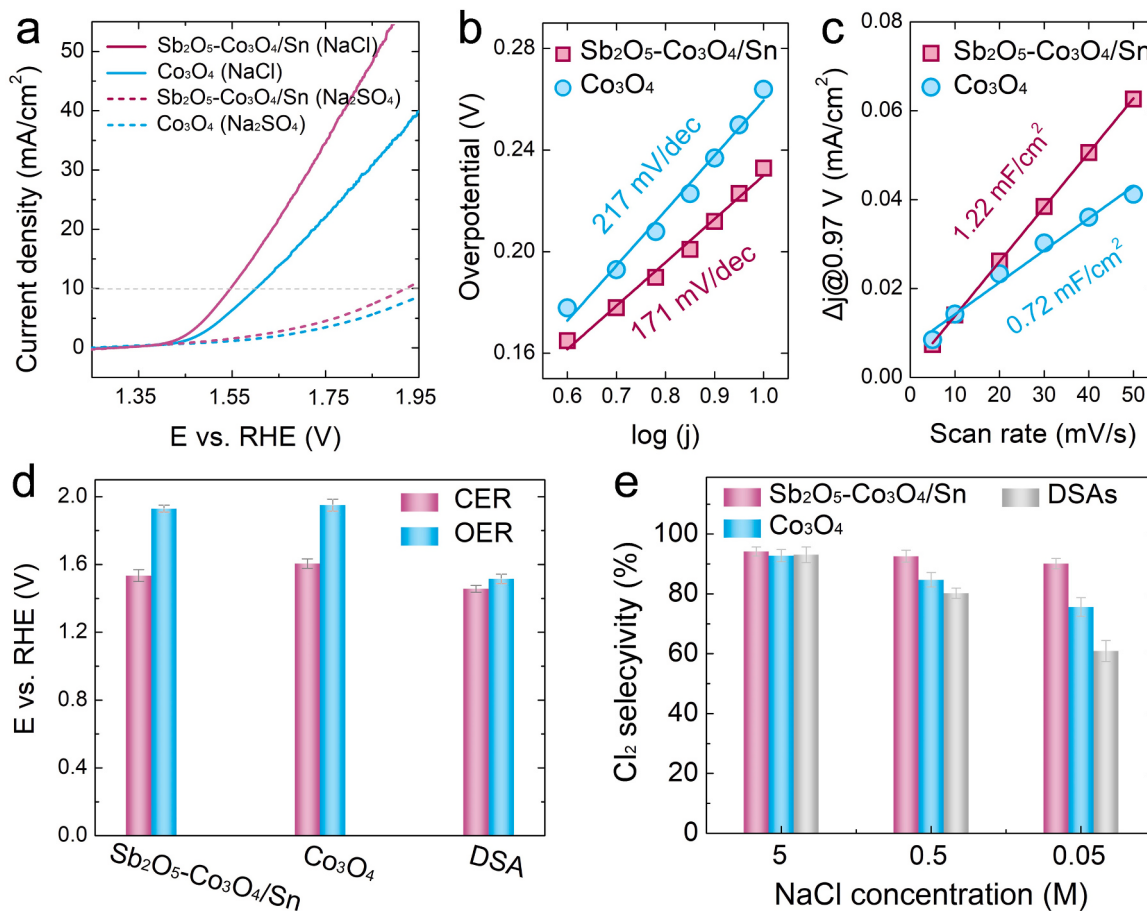


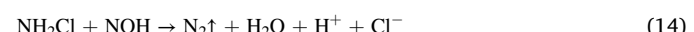
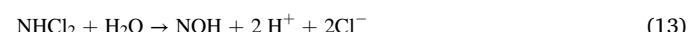
Fig. 3. (a) LSV curves of $\text{Sb}_2\text{O}_5\text{-Co}_3\text{O}_4/\text{Sn}$ and Co_3O_4 electrodes with saturated electrolytes. Conditions: $[\text{NaCl}] = 5 \text{ M}$, $[\text{Na}_2\text{SO}_4] = 2 \text{ M}$; (b) Tafel slopes of $\text{Sb}_2\text{O}_5\text{-Co}_3\text{O}_4/\text{Sn}$ and Co_3O_4 anodes. Conditions: $[\text{NaCl}] = 5 \text{ M}$; (c) Electrochemical double-layer capacitance (C_{dl}) of $\text{Sb}_2\text{O}_5\text{-Co}_3\text{O}_4/\text{Sn}$ and Co_3O_4 electrodes at the potential of 0.97 V vs. RHE. Conditions: $[\text{NaCl}] = 5 \text{ M}$; (d) Chlorine evolution and oxygen evolution potentials (vs. RHE) of different saturated electrodes at a current density of 10 mA/cm^2 . Conditions: $[\text{NaCl}] = 5 \text{ M}$, $[\text{Na}_2\text{SO}_4] = 2 \text{ M}$; (e) Comparison of the CER activity and selectivity of different anodes with different electrolyte concentrations. Conditions: current density = 10 mA/cm^2 , pH = 6.

raw Co_3O_4 anode and commercial DSAs.

3.2.2. Determination of active species

Free radical quenching experiments are performed to identify the active species involved during the ammonia removal process. NB is utilized as the scavenger for $\cdot\text{OH}$ ($k(\text{NB}, \cdot\text{OH}) = 3.9 \times 10^9 \text{ M}^{-1}\text{s}^{-1}$), TBA as the scavenger for $\cdot\text{OH}$ ($k(\text{TBA}, \cdot\text{OH}) = 6.0 \times 10^8 \text{ M}^{-1}\text{s}^{-1}$), Cl^\bullet ($k(\text{TBA}, \text{Cl}^\bullet) = 3.0 \times 10^8 \text{ M}^{-1}\text{s}^{-1}$), ClO^\bullet ($k(\text{TBA}, \text{ClO}^\bullet) = 1.3 \times 10^7 \text{ M}^{-1}\text{s}^{-1}$), and CBZ as the scavenger for $\cdot\text{OH}$ ($k(\text{HO}^\bullet, \text{CBZ}) = 8.8 \times 10^9 \text{ M}^{-1}\text{s}^{-1}$), Cl^\bullet ($k(\text{Cl}^\bullet, \text{CBZ}) = 3.3 \times 10^{10} \text{ M}^{-1}\text{s}^{-1}$), ClO^\bullet ($k(\text{ClO}^\bullet, \text{CBZ}) = 1.97 \times 10^8 \text{ M}^{-1}\text{s}^{-1}$), and Cl_2^\bullet ($k(\text{Cl}_2^\bullet, \text{CBZ}) = 4.3 \times 10^7 \text{ M}^{-1}\text{s}^{-1}$) respectively [41–44]. As demonstrated in Fig. 2c, the removal of ammonia is inappreciably inhibited with the addition of excess scavengers, indicating that $\cdot\text{OH}$, $\cdot\text{Cl}$, ClO^\bullet and Cl_2^\bullet do not dedicate to the ammonia removal in the EC system. Besides, EPR spectra is further used to exploit the presence of $\cdot\text{OH}$, $\cdot\text{Cl}$, ClO^\bullet and Cl_2^\bullet . As illustrated in Fig. 2d, merely the characteristic peaks of adduct-products of 5,5-dimethyl-1-pyrroline N-oxide (DMPO) and $\cdot\text{Cl}$ are observed and the peak intensity is negligible [25]. It is known that the formation of Cl_2 is derived from the self-quenching of $\cdot\text{Cl}$ (Eqs. 4–7). The generated $\cdot\text{Cl}$ could be quickly converted into Cl_2 and does not contribute to the ammonia removal. Moreover, the concentration variation of free chlorines (Cl_2 , HClO , and ClO^\bullet) during the ammonia removal process is further quantified. As exhibited in Fig. S14, the concentration of free chlorine is much lower than 0.5 mg/L within 90 min in the EC system with $\text{Sb}_2\text{O}_5\text{-Co}_3\text{O}_4/\text{Sn}$ anode because the free chlorines are continuously consumed by

ammonia. After the complete elimination of ammonia ($> 90 \text{ min}$), free chlorines are no longer consumed and their concentrations increase observably. Similar phenomena are observed in the EC system with Co_3O_4 anode or DSAs. Based on the above results, the dominant species for ammonia removal in the EC system is attributed to the free chlorine, which can efficiently and selectively oxidize ammonia into N_2 (Eqs. 8–14) [45].



3.3. Enhanced mechanism of ammonia removal

3.3.1. CER activity and selectivity of $\text{Sb}_2\text{O}_5\text{-Co}_3\text{O}_4/\text{Sn}$ anode

The CER activity and selectivity of the $\text{Sb}_2\text{O}_5\text{-Co}_3\text{O}_4/\text{Sn}$ anode are investigated thoroughly by varied electrochemical characterizations. As

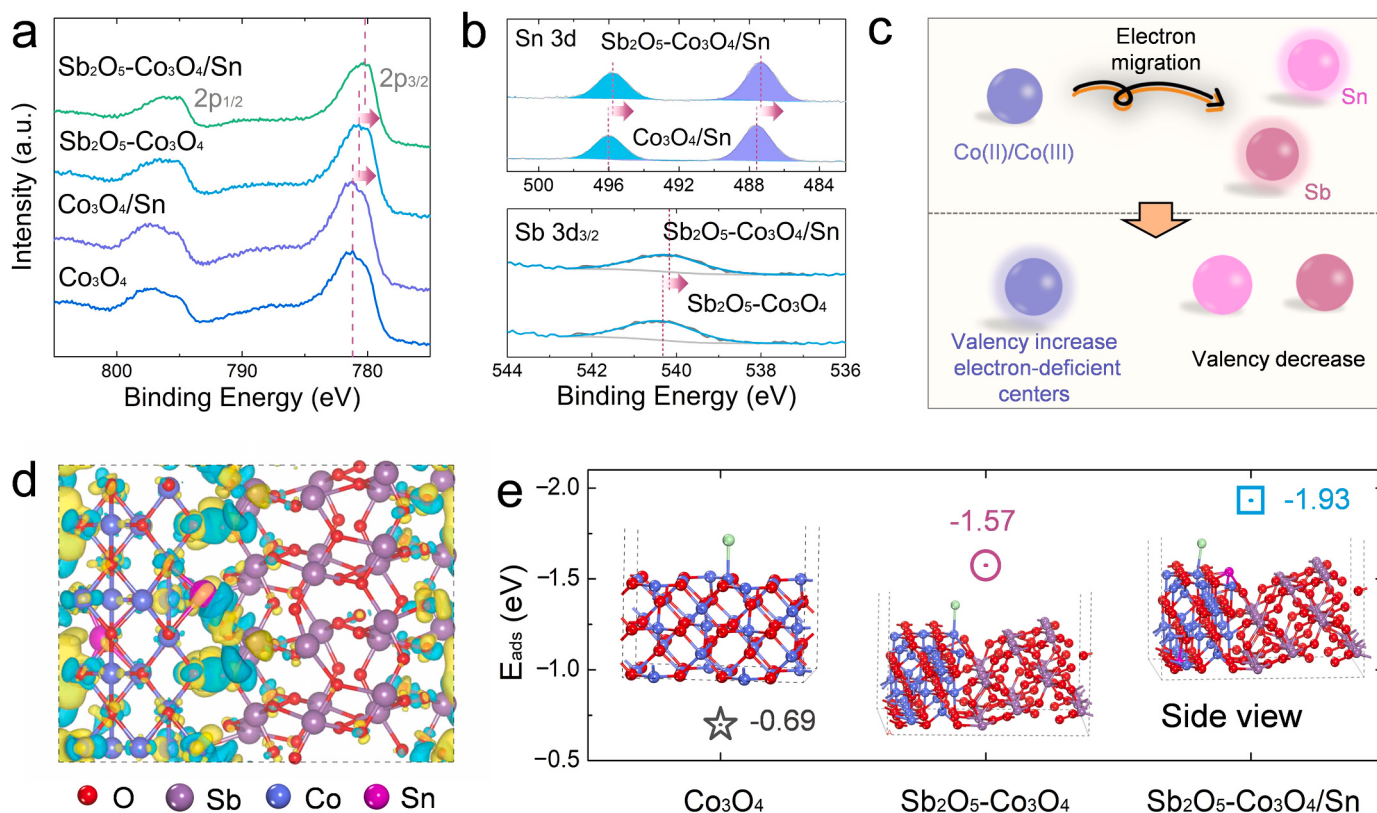


Fig. 4. (a) XPS spectra of Co 2p orbitals before and after Co₃O₄ modification; (b) XPS spectra of Sb 3d_{3/2} and Sn 3d orbitals of Sb₂O₅-Co₃O₄, Co₃O₄/Sn and Sb₂O₅-Co₃O₄/Sn; (c) Schematic diagram of electron migration between Co(II)/Co(III) and Sn/Sb; (d) Difference charge density image of Sb₂O₅-Co₃O₄/Sn; (e) Adsorption energy between Cl⁻ and the structural Co(III) in the Co₃O₄, Sb₂O₅-Co₃O₄ and Sb₂O₅-Co₃O₄/Sn electrodes.

exhibited in Fig. 3a, when the saturated NaCl solution (5 M) is used as the electrolyte, a higher current density is observed in the linear sweep voltammetry (LSV) curves with Sb₂O₅-Co₃O₄/Sn anode than that with Co₃O₄ anode, indicating that the introduction of Sn and Sb into Co₃O₄ efficiently enhances its CER activity. Besides, the Tafel slope of Sb₂O₅-Co₃O₄/Sn under 5 M NaCl electrolyte is 171 mV/dec, much lower than that of Co₃O₄ anode (217 mV/dec) (Fig. 3b). Due to a smaller Tafel slope, the CER kinetics of Sb₂O₅-Co₃O₄/Sn anode is much stronger than Co₃O₄ anode. Moreover, the electrochemical surface area (ECSA) of the Sb₂O₅-Co₃O₄/Sn and Co₃O₄ electrode is explored by the electrochemical double-layer capacitance (C_{dl}) to compare their intrinsic activities [46]. As exhibited in Fig. 3c, S15, and S16, the C_{dl} value and intrinsic activity of the Sb₂O₅-Co₃O₄/Sn anode are much higher than that of the Co₃O₄ anode, further proving the improvement of CER activity after the introduction of Sb and Sn into Co₃O₄.

In addition, the potentials of CER and oxygen evolution reaction (OER) of Sb₂O₅-Co₃O₄/Sn anode at 10 mA/cm² are 1.52 and 1.92 V vs. RHE, respectively (Fig. 3d). As a comparison, the CER and OER potentials of Co₃O₄ anode are 1.61 and 1.96 V vs. RHE, respectively. Benefiting from the lower CER potential and a larger difference between CER and OER potentials, the Sb₂O₅-Co₃O₄/Sn anode has more exceptional CER activity and selectivity than the Co₃O₄ anode. Noteworthily, as for the commercial DSAs, though it has strong CER kinetics and a large active area (Figs. S17 – S19), the close potentials of CER (1.46 V vs. RHE) and OER (1.52 V vs. RHE) could cause severe side reaction of oxygen evolution (Fig. 3d) and inhibit the CER selectivity. Finally, the CER selectivity of different anodes is further compared at 10 mA/cm². As illustrated in Fig. 3e, the CER selectivity of anodes increases with the increase of NaCl concentrations. More importantly, when NaCl concentration is 50 mM, the CER selectivity of Sb₂O₅-Co₃O₄/Sn is 90.1%, far higher than that of Co₃O₄ (75.6%), and commercial DSAs (60.9%). It is because the formation of Co(III) electron-deficient centers in Sb₂O₅-Co₃O₄/Sn.

Co₃O₄/Sn effectively enhance the enrichment of Cl⁻, which accelerates the diffusion of Cl⁻ from solution to anodic active sites, further promoting the CER selectivity. Based on the above results, it can be concluded that the CER activity and selectivity of the Co₃O₄ anode are effectively improved after the introduction of Sb and Sn, which is in favor of the removal of ammonia.

3.3.2. Enhanced enrichment mechanism of Cl⁻ at Co(III)

By comparing the electronic structure of Co(III) sites and their binding ability with Cl⁻ in the different electrodes, the enhanced mechanism of ammonia removal in the EC system with Sb₂O₅-Co₃O₄/Sn anode is deeply explored. Normally, the shift of the binding energy in XPS spectra towards the lower value indicates that the atom has gained electrons [47], but the peculiarity of the cobalt makes it quite the opposite [48]. As illustrated in Fig. 4a, the binding energy of the Co 2p_{1/2} and Co 2p_{3/2} orbitals of Co₃O₄ before and after doping of Sn is invariable, indicating that no electron migration occurs between Co(II)/Co(III) and Sn. Besides, when Sb₂O₅ is compounded with Co₃O₄, the binding energy of Co 2p_{1/2} and Co 2p_{3/2} orbitals decreases significantly from 796.7 and 781.4 eV to 795.9 and 780.6 eV, respectively. This phenomenon indicates that the electron cloud around Co(II)/Co(III) in Co₃O₄ shifted toward Sb, leading to the formation of Co(III) with electron-deficient centers. Moreover, after the further doping of Sn into Sb₂O₅-Co₃O₄, the binding energy of Co 2p_{1/2} and Co 2p_{3/2} orbitals further decreased to 795.4 and 780.1 eV, showing more robust electron-deficient centers of Co(II)/Co(III) formed in Sb₂O₅-Co₃O₄/Sn than that in Sb₂O₅-Co₃O₄. The simultaneous introduction of Sn and Sb into Co₃O₄ synergistically strengthens the construction of Co(III) with electron-deficient centers. In addition, compared with Sb₂O₅-Co₃O₄ and Co₃O₄/Sn, the binding energy of Sb 3d and Sn 3d orbitals decreases (Fig. 4b) in Sb₂O₅-Co₃O₄/Sn. Thus, the introduction of Sb and Sn into Co₃O₄ cause the electron cloud around Co migration to Sn and Sb, which

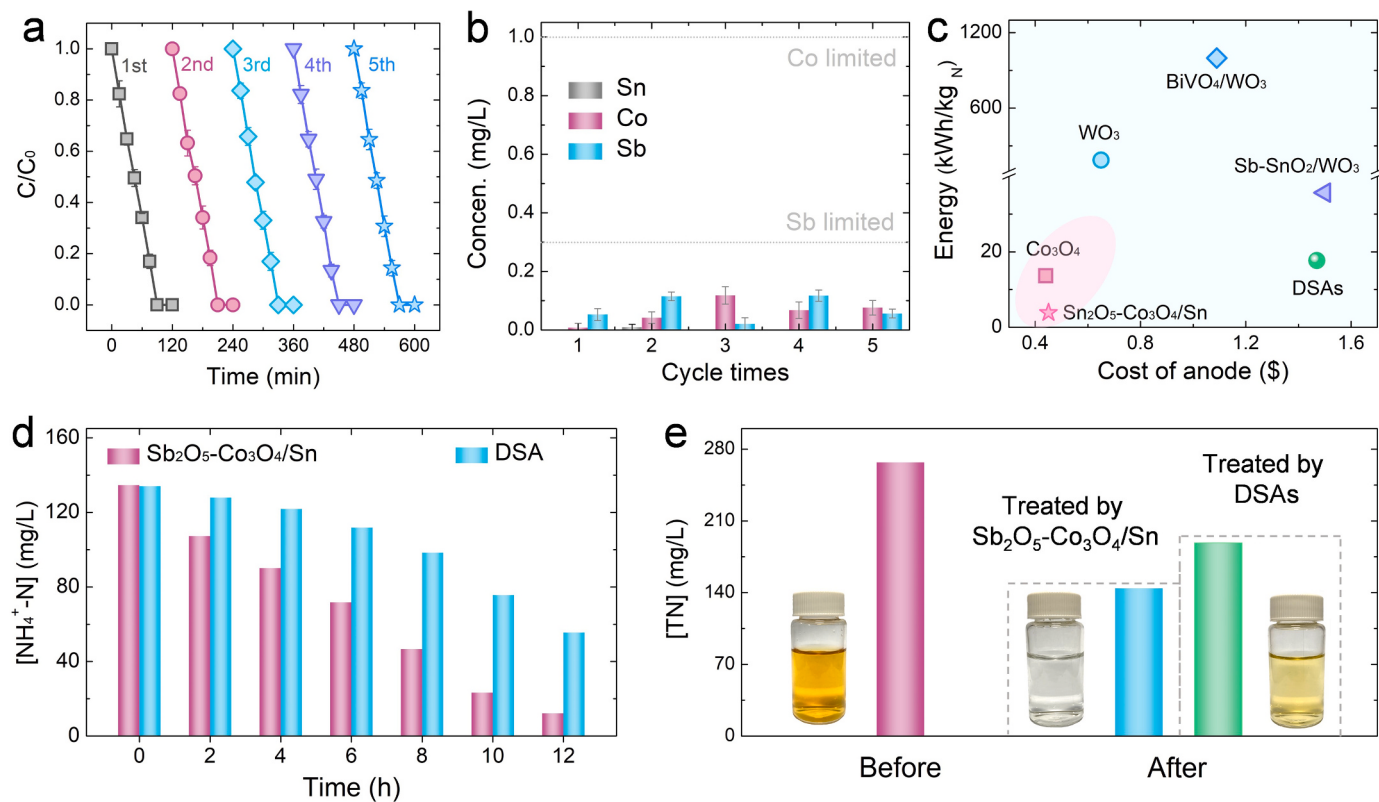


Fig. 5. (a) Ammonia removal performance with $\text{Sb}_2\text{O}_5\text{-Co}_3\text{O}_4\text{/Sn}$ anode within five cycles; (b) Ion leaching concentration during the five cycles process; (c) Cost analysis of different systems for ammonia removal; (d) Ammonia removal in the treatment of practical wastewater by $\text{Sb}_2\text{O}_5\text{-Co}_3\text{O}_4\text{/Sn}$ and DSAs in the EC system; (e) TN and color change of pickle wastewater before and after treated with $\text{Sb}_2\text{O}_5\text{-Co}_3\text{O}_4\text{/Sn}$ or DSAs electrode. Conditions: $[\text{NH}_4^+ \text{-N}] = 50 \text{ mg/L}$, $[\text{NaCl}] = 50 \text{ mM}$, $\text{pH} = 6$, $[\text{scavengers}] = 10 \text{ mM}$, constant current = 20 mA.

is governed by electronegativity. The schematic diagram of electron migration between Co(II)/Co(III), Sn, and Sb is exhibited in Fig. 4c. In conclusion, with the simultaneous introduction of Sb and Sn into Co_3O_4 , the synergy between Sb and Sn can efficiently induce the formation of Co(III) sites with strong electron-deficient centers, which is in favor of the enrichment of Cl^- , and further facilitating the CER activity and selectivity of $\text{Sb}_2\text{O}_5\text{-Co}_3\text{O}_4\text{/Sn}$ anode.

The differential charge density of the different anodes is analyzed by DFT to further verify the electronic structure of Co(III) sites. The yellow color is the accumulation region of electrons and the blue color is the dissipation region of electrons. As exhibited in Fig. S20, when Sb_2O_5 is compounded with Co_3O_4 , an obvious electron migration from Co(III) to Sb atom is observed because the districts around Co and Sb are blue and yellow, respectively. As a comparison, after the simultaneous introduction of Sb and Sn into Co_3O_4 , the density of electron cloud around Co (III) in $\text{Sb}_2\text{O}_5\text{-Co}_3\text{O}_4\text{/Sn}$ (blue area) is significantly lower than that in $\text{Sb}_2\text{O}_5\text{-Co}_3\text{O}_4$ (Fig. 4d). As a result, the electron migration of Co(III) in $\text{Sb}_2\text{O}_5\text{-Co}_3\text{O}_4\text{/Sn}$ is more significant than that in $\text{Sb}_2\text{O}_5\text{-Co}_3\text{O}_4$ and the electron-deficient centers of Co(III) in the $\text{Sb}_2\text{O}_5\text{-Co}_3\text{O}_4\text{/Sn}$ anode are further enhanced after the simultaneous introduction of Sb and Sn. In addition, the adsorption energy (E_{ads}) between Co(III) in Co_3O_4 before and after modification and Cl^- is calculated by DFT. As illustrated in Fig. 4d and S21, E_{ads} between Co(III) and Cl^- is much higher than that of other sites (such as Co(II), Sb, Sn, and O), indicating Co(III) is the dominant site for Cl^- enrichment and activation. After the introduction of Sb and Sn, E_{ads} between Co(III) in the anodes of $\text{Sb}_2\text{O}_5\text{-Co}_3\text{O}_4$ and $\text{Sb}_2\text{O}_5\text{-Co}_3\text{O}_4\text{/Sn}$ and Cl^- markedly increases from -0.69 eV to -1.57 and -1.93 eV , respectively. The simultaneous introduction of Sb and Sn into Co_3O_4 immensely promotes the binding ability of structural Co(III) and Cl^- , thereby improving the CER activity and selectivity and ammonia removal performance.

Based on the above results, the enhanced mechanism of ammonia removal in the EC system with $\text{Sb}_2\text{O}_5\text{-Co}_3\text{O}_4\text{/Sn}$ anode can be summarized as follows. Benefiting from the high electronegativity, the introduction of Sn and Sb into Co_3O_4 can synergistically induce the construction of strong electron-deficient centers of Co(III) sites. The binding ability between the structural Co(III) in the anode and Cl^- is strengthened, leading to the enhancement of the CER activity and selectivity. Therefore, the efficient mineralization of ammonia into N_2 by free chlorines is realized in the EC system with $\text{Sb}_2\text{O}_5\text{-Co}_3\text{O}_4\text{/Sn}$ anode.

3.4. Practical application

To evaluate the practical application of the $\text{Sb}_2\text{O}_5\text{-Co}_3\text{O}_4\text{/Sn}$ electrode, five cycles of experiments are carried out. As shown in Fig. 5a and S22, there is no inhibition of ammonia elimination observed in each cycle, and nearly 100% of ammonia is mineralized into N_2 after 5 cycles. Besides, the dissolution concentrations of different metal ions after each cycle are measured. As demonstrated in Fig. 5b, when $\text{Sb}_2\text{O}_5\text{-Co}_3\text{O}_4\text{/Sn}$ is used as the anode, the antimony ion concentrations are all less than 0.15 mg/L , and almost no stannum ions are detected during the cycle process. More importantly, the concentration of cobalt ions is less than 0.1 mg/L in each cycle, which is much lower than that of the raw Co_3O_4 anode (1.3 mg/L). Moreover, there is no difference in the morphology and structure of the $\text{Sb}_2\text{O}_5\text{-Co}_3\text{O}_4\text{/Sn}$ anode before and after 5 cycles (Figs. S23 – S25). In addition, the LSV curves of $\text{Sb}_2\text{O}_5\text{-Co}_3\text{O}_4\text{/Sn}$ anode before and after 5 cycles are almost completely coincident and there is no obvious increased potential observed in the long-term durability test for 24 h (Figs. S26 and S27). In conclusion, the $\text{Sb}_2\text{O}_5\text{-Co}_3\text{O}_4\text{/Sn}$ electrode has excellent stability and shows good application potential in the treatment of ammonia-containing wastewater.

Table 1

Contents of practical pickle wastewater before and after treated by $\text{Sb}_2\text{O}_5\text{-Co}_3\text{O}_4\text{/Sn}$.

Indicators	$\text{NH}_4^+\text{-N}$ (mg/L)	TN (mg/L)	Salinity (%)	pH
Raw water	135	268	4–10	5.0
Treated water	12	151	4–10	4.7

To further explore the feasibility of practical applications of the $\text{Sb}_2\text{O}_5\text{-Co}_3\text{O}_4\text{/Sn}$ anode, the cost analysis for ammonia removal is performed. As presented in **Fig. 5c** and Table S2, no matter the electrode cost or the required energy consumption, the cost of the $\text{Sb}_2\text{O}_5\text{-Co}_3\text{O}_4\text{/Sn}$ anode (0.45 \$/piece; 3.9 kWh/kg-N) is much lower than DSAs (1.47 \$/piece; 17.7 kWh/kg-N) and other anodes reported by other investigators [11,45,49]. This result preliminarily reveals that $\text{Sb}_2\text{O}_5\text{-Co}_3\text{O}_4\text{/Sn}$ anode has good feasibility in the treatment of ammonia. Subsequently, the EC system with $\text{Sb}_2\text{O}_5\text{-Co}_3\text{O}_4\text{/Sn}$ anode is employed to treat the practical pickle wastewater with a high concentration of ammonia. The main components of pickle wastewater are exhibited in **Table 1**. As demonstrated in **Fig. 5d**, when $\text{Sb}_2\text{O}_5\text{-Co}_3\text{O}_4\text{/Sn}$ is used as the anode, the concentration of ammonia-nitrogen reduces from 135 mg/L to 12 mg/L within 12 h, and 88.9% of ammonia can be eliminated, which is much superior to that with DSAs (58.8%). Correspondingly, the color of the wastewater after 12 h treatment with $\text{Sb}_2\text{O}_5\text{-Co}_3\text{O}_4\text{/Sn}$ anodes changes to colorless, while changes to pale-yellow with the DSAs electrode (**Fig. 5e**). Since the decrease in total nitrogen concentration is close to that of the decrease of ammonia-nitrogen (**Figs. 5d** and **5e**), ammonia is efficiently mineralized into N_2 in the EC system. In summary, $\text{Sb}_2\text{O}_5\text{-Co}_3\text{O}_4\text{/Sn}$ anode shows exceptional feasibility and potential for the treatment of practical ammonia-containing wastewater.

4. Conclusion

This study constructs a novel $\text{Sb}_2\text{O}_5\text{-Co}_3\text{O}_4\text{/Sn}$ anode with high CER activity and selectivity, in which robust electron-deficient centers of Co (III) sites are formed after the introduction of strongly electronegative Sb and Sn to enhance the enrichment of Cl^- . The results of experiments and characterizations reveal that Sb_2O_5 is compounded with Co_3O_4 , while Sn (IV) dopes into tetrahedral Co(II) sites of Co_3O_4 . The binding capacity (E_{ads}) between Cl^- and Co(III) sites is strengthened from -0.69 eV to -1.93 eV and the potential difference between CER and OER is widened, further promoting the CER activity and selectivity (90.1%). Besides, 50 mg/L of ammonia-nitrogen can be efficiently mineralized into N_2 within 90 min with low energy consumption (3.9 kWh/kg-N) in the EC system with $\text{Sb}_2\text{O}_5\text{-Co}_3\text{O}_4\text{/Sn}$ anode, which is far superior to that of the commercial DSAs (17.7 kWh/kg-N). Finally, 88.9% of ammonia in the pickle wastewater is mineralized within 12 h in this EC system, which exhibits its exceptional feasibility of practical ammonia-containing wastewater treatment. This study provides a new design thought to construct electrode materials with high activity and selectivity of CER for the efficient treatment of ammonia-containing wastewater.

CRediT authorship contribution statement

Lei Tian: Investigation, Formal analysis, Conceptualization, Writing – original draft, Writing – review & editing. **Xing-Yuan Xia:** Investigation, Formal analysis. **Li-Juan Zhou:** Investigation, Formal analysis. **Ling-Ling Zheng:** Data curation. **Qiu-Ju Xing:** Formal analysis. **Long-Shuai Zhang:** Supervision. **Jian-Ping Zou:** Conceptualization, Methodology, Resources, Supervision, Writing – review & editing, Resources, Project administration. **Zhao-Qing Liu:** Conceptualization, Methodology.

Declaration of Competing Interest

The authors declare that they have no known competing financial interests or personal relationships that could have appeared to influence the work reported in this paper.

Data availability

Data will be made available on request.

Acknowledgements

We gratefully acknowledge the financial support of the National Natural Science Foundation of China (52170082, 51878325, 51938007, and 52100186), and the Natural Science Foundation of Jiangxi Province (20212ACB203008).

Appendix A. Supporting information

Supplementary data associated with this article can be found in the online version at doi:10.1016/j.apcatb.2023.123260.

References

- [1] M.R. Adam, M.H.D. Othman, R.A. Samah, M.H. Puteh, A.F. Ismail, A. Mustafa, M. A. Rahman, J. Jaafar, Current trends and future prospects of ammonia removal in wastewater: a comprehensive review on adsorptive membrane development, *Sep. Purif. Technol.* 213 (2019) 114–132, <https://doi.org/10.1016/j.seppur.2018.12.030>.
- [2] B. Han, C. Butterly, W. Zhang, J.Z. He, D.L. Chen, Adsorbent materials for ammonium and ammonia removal: a review, *J. Clean. Prod.* 283 (2021), 124611, <https://doi.org/10.1016/j.jclepro.2020.124611>.
- [3] L. Li, Y. Liu, Ammonia removal in electrochemical oxidation: mechanism and pseudo-kinetics, *J. Hazard. Mater.* 161 (2009) 1010–1016, <https://doi.org/10.1016/j.jhazmat.2008.04.047>.
- [4] P.Y. Jiang, T.S. Zhou, J. Bai, Y. Zhang, J.H. Li, C.H. Zhou, B.X. Zhou, Nitrogen-containing wastewater fuel cells for total nitrogen removal and energy recovery based on $\text{Cl}\bullet/\text{ClO}\bullet$ oxidation of ammonia nitrogen, *Water Res* 235 (2023), 119914, <https://doi.org/10.1016/j.watres.2023.119914>.
- [5] J.W. Hao, S. Zhao, R. Mao, X. Zhao, Activation of peroxyomonosulfate by cobalt doped graphitic carbon nitride for ammonia removal in chloride-containing wastewater, *Sep. Purif. Technol.* 271 (2021), 118858, <https://doi.org/10.1016/j.seppur.2021.118858>.
- [6] Z.C. Liu, G. Zhang, H.C. Lan, H.J. Liu, J.H. Qu, Optimization of a hierarchical porous-structured reactor to mitigate mass transport limitations for efficient electrocatalytic ammonia oxidation through a three-electron-transfer pathway, *Environ. Sci. Technol.* 55 (2021) 12596–12606, <https://doi.org/10.1021/acs.est.1c02825>.
- [7] H. Huang, H.C. Zheng, J.J. Jiao, Y. Lei, Y.J. Zhou, J.L. Qiu, X. Yang, Trichloramine and hydroxyl radical contributions to dichloroacetonitrile formation following breakpoint chlorination, *Environ. Sci. Technol.* 56 (2022) 12592–12601, <https://doi.org/10.1021/acs.est.2c03701>.
- [8] C. Jantarakasem, I. Kasuga, F. Kurisu, H. Furumai, Temperature-dependent ammonium removal capacity of biological activated carbon used in a full-scale drinking water treatment plant, *Environ. Sci. Technol.* 54 (2020) 13257–13263, <https://doi.org/10.1021/acs.est.0c02502>.
- [9] T.A. Pressley, D.F. Bishop, S.G. Roan, Ammonia-nitrogen removal by breakpoint chlorination, *Environ. Sci. Technol.* 6 (1972) 622–628, <https://doi.org/10.1021/es60066a006>.
- [10] X.R. Zhang, W.G. Li, E.R. Blatchley III, X.J. Wang, P.F. Ren, UV/chlorine process for ammonia removal and disinfection by-product reduction: comparison with chlorination, *Water Res* 68 (2015) 804–811, <https://doi.org/10.1016/j.watres.2014.10.044>.
- [11] Y.Z. Ji, J. Bai, J.H. Li, T. Luo, L. Qiao, Q.Y. Zeng, B.X. Zhou, Highly selective transformation of ammonia nitrogen to N_2 based on a novel solar-driven photoelectrocatalytic-chlorine radical reactions system, *Water Res* 125 (2017) 512–519, <https://doi.org/10.1016/j.watres.2017.08.053>.
- [12] F. Li, L.W. Sun, Y.B. Liu, X.F. Fang, C.S. Shen, M.H. Huang, Z.W. Wang, D. D. Dionysiou, A $\text{ClO}\bullet$ -mediated photoelectrochemical filtration system for highly-efficient and complete ammonia conversion, *J. Hazard. Mater.* 400 (2020), 123246, <https://doi.org/10.1016/j.jhazmat.2020.123246>.
- [13] C.Y. Zhang, D. He, J.X. Ma, T.D. Waite, Active chlorine mediated ammonia oxidation revisited: reaction mechanism, kinetic modelling and implications, *Water Res* 145 (2018) 220–230, <https://doi.org/10.1016/j.watres.2018.08.025>.
- [14] Y. Chen, G. Zhang, Q.H. Ji, H.C. Lan, H.J. Liu, J.H. Qu, Visualization of electrochemically accessible sites in flow-through mode for maximizing available active area toward superior electrocatalytic ammonia oxidation, *Environ. Sci. Technol.* 56 (2022) 9722–9731, <https://doi.org/10.1021/acs.est.2c01707>.

[15] Y.Y. Liu, C. Li, C.H. Tan, Z.X. Pei, T. Yang, S.Z. Zhang, Q.W. Huang, Y.H. Wang, Z. Zhou, X.Z. Liao, J.C. Dong, H. Tan, W.S. Yan, H.J. Yin, Z.Q. Liu, J. Huang, S. L. Zhao, Electrosynthesis of chlorine from seawater-like solution through single-atom catalysts, *Nat. Commun.* 14 (2023) 2475, <https://doi.org/10.1038/s41467-023-38129-w>.

[16] J.J. Zhou, F. Pan, Q.F. Yao, Y.Q. Zhu, H.R. Ma, J.F. Niu, J.P. Xie, Achieving efficient and stable electrochemical nitrate removal by in-situ reconstruction of $\text{Cu}_2\text{O}/\text{Cu}$ electroactive nanocatalysts on Cu foam, *Appl. Catal. B: Environ.* 317 (2022), 121811, <https://doi.org/10.1016/j.apcatb.2022.121811>.

[17] S.X. Li, Y.B. Tong, H.Y. Dong, J.J. Lu, J.F. Niu, Formation of stable imine intermediates in the coexistence of sulfamethoxazole and humic acid by electrochemical oxidation, *J. Hazard. Mater.* 427 (2022), 128166, <https://doi.org/10.1016/j.jhazmat.2021.128166>.

[18] H. Lin, J.F. Niu, S.Y. Ding, L.L. Zhang, Electrochemical degradation of perfluorooctanoic acid (PFOA) by $\text{Ti}/\text{SnO}_2\text{-Sb}$, $\text{Ti}/\text{SnO}_2\text{-Sb}/\text{PbO}_2$ and $\text{Ti}/\text{SnO}_2\text{-Sb}/\text{MnO}_2$ anodes, *Water Res* 46 (2012) 2281–2289, <https://doi.org/10.1016/j.watres.2012.01.053>.

[19] T. Lim, G.Y. Jung, J.H. Kim, S.O. Park, J. Park, Y.T. Kim, S.J. Kang, H.Y. Jeong, S. K. Kwak, S.H. Joo, Atomically dispersed Pt–N₄ sites as efficient and selective electrocatalysts for the chlorine evolution reaction, *Nat. Commun.* 11 (2020) 412, <https://doi.org/10.1038/s41467-019-14272-1>.

[20] T. Lim, J.H. Kim, J. Kim, D.S. Baek, T.J. Shin, H.Y. Jeong, K.S. Lee, K.S. Exner, S. H. Joo, General efficacy of atomically dispersed Pt catalysts for the chlorine evolution reaction: potential-dependent switching of the kinetics and mechanism, *ACS Catal.* 11 (2021) 12232–12246, <https://doi.org/10.1021/acscatal.1c03893>.

[21] Y.C. Yao, L. Zhao, J. Dai, J.X. Wang, C.Y. Fang, G.M. Zhan, Q. Zheng, W. Hou, L. Z. Zhang, Single atom Ru monolithic electrode for efficient chlorine evolution and nitrate reduction, *Angew. Chem. Int. Ed.* 61 (2022), e202208215, <https://doi.org/10.1002/anie.202208215>.

[22] X. Zhang, D. Wu, X. Liu, Y. Qiu, Z. Liu, H. Xie, J. Duan, B. Hou, Efficient electrocatalytic chlorine evolution under neutral seawater conditions enabled by highly dispersed Co_3O_4 catalysts on porous carbon, *Appl. Catal. B: Environ.* 330 (2023), 122597, <https://doi.org/10.1016/j.apcatb.2023.122597>.

[23] X.L. Zhu, P. Wang, Z.Y. Wang, Y.Y. Liu, Z.K. Zheng, Q.Q. Zhang, X.Y. Zhang, Y. Dai, M.H. Whangbo, B.B. Huang, Co_3O_4 nanobelts arrays assembled with ultrathin nanosheets as highly efficient and stable electrocatalysts for the chlorine evolution reaction, *J. Mater. Chem. A* 6 (2018) 12718–12723, <https://doi.org/10.1039/C8TA03689F>.

[24] Y. Zhang, W.J. Tang, J. Bai, J.H. Li, J.C. Wang, T.S. Zhou, X.H. Guan, B.X. Zhou, Highly efficient removal of total nitrogen and dissolved organic compound in waste reverse osmosis concentrate mediated by chlorine radical on 3D Co_3O_4 nanowires anode, *J. Hazard. Mater.* 424 (2022), 127662, <https://doi.org/10.1016/j.jhazmat.2021.127662>.

[25] Y. Zhang, X.Y. Huang, J.H. Li, J. Bai, G.H. Zhou, L. Li, J.C. Wang, M.C. Long, X. Y. Zhu, B.X. Zhou, Rapid conversion of Co^{2+} to Co^{3+} by introducing oxygen vacancies in Co_3O_4 nanowire anodes for nitrogen removal with highly efficient H₂ recovery in urine treatment, *Environ. Sci. Technol.* 56 (2022) 9693–9701, <https://doi.org/10.1021/acs.est.2c00729>.

[26] Z.P. Wang, P.Y. Wu, X.B. Zou, S. Wang, L. Du, T. Ouyang, Z.Q. Liu, Optimizing the oxygen-catalytic performance of Zn–Mn–Co spinel by regulating the bond competition at octahedral sites, *Adv. Funct. Mater.* 33 (2023) 2214275, <https://doi.org/10.1002/adfm.202214275>.

[27] W.J. Duan, G. Li, Z.C. Lei, T.G. Zhu, Y.Z. Xue, C.H. Wei, C.H. Feng, Highly active and durable carbon electrocatalyst for nitrate reduction reaction, *Water Res* 161 (2019) 126–135, <https://doi.org/10.1016/j.watres.2019.05.104>.

[28] H. Wang, Z. Han, Y. Zhou, X. Liu, D. Zeng, W. Wang, D. Sarker, L. Zhang, W. Wang, Efficient photocatalytic chlorine production on bismuth oxychloride in chloride solution, *Appl. Catal. B: Environ.* 297 (2021), 120436, <https://doi.org/10.1016/j.apcatb.2021.120436>.

[29] A.D. Jagadale, V.S. Kumbhar, C.D. Lokhande, Supercapacitive activities of potentiodynamically deposited nanoflakes of cobalt oxide (Co_3O_4) thin film electrode, *J. Colloid Interface Sci.* 406 (2013) 225–230, <https://doi.org/10.1016/j.jcis.2013.05.037>.

[30] Y. Wang, C.M. Yang, W. Schmidt, B. Spliethoff, E. Bill, F. Schüth, Weakly ferromagnetic ordered mesoporous Co_3O_4 synthesized by nanocasting from vinyl-functionalized cubic Ia3d mesoporous silica, *Adv. Mater.* 17 (2005) 53–56, <https://doi.org/10.1002/adma.200400777>.

[31] J.P. Zou, Y. Chen, S.S. Liu, Q.J. Xing, W.H. Dong, X.B. Luo, W.L. Dai, X. Xiao, J. M. Luo, J. Crittenden, Electrochemical oxidation and advanced oxidation processes using a 3D hexagonal Co_3O_4 array anode for 4-nitrophenol decomposition coupled with simultaneous CO₂ conversion to liquid fuels via a flower-like CuO cathode, *Water Res* 150 (2019) 330–339, <https://doi.org/10.1016/j.watres.2018.11.077>.

[32] X. Chen, B. Liu, C. Zhong, Z. Liu, J. Liu, L. Ma, Y.D. Deng, X.P. Han, T.P. Wu, W. B. Hu, J. Lu, Ultrathin Co_3O_4 layers with large contact area on carbon fibers as high-performance electrode for flexible zinc-air battery integrated with flexible display, *Adv. Energy Mater.* 7 (2017) 1700779, <https://doi.org/10.1002/aenm.201700779>.

[33] H.L. Jiang, L. Tian, P.H. Chen, Y.C. Bai, X.Q. Li, H.Y. Shu, X.B. Luo, Efficient antimony removal by self-assembled core-shell nanocomposite of $\text{Co}_3\text{O}_4@r\text{GO}$ and the analysis of its adsorption mechanism, *Environ. Res.* 187 (2020), 109657, <https://doi.org/10.1016/j.envres.2020.109657>.

[34] J.P. Correa-Baena, K. Artyushkova, C. Santoro, P. Atanassov, A.G. Agrios, Morphological characterization of ALD and doping effects on mesoporous SnO_2 aerogels by XPS and quantitative SEM image analysis, *ACS Appl. Mater. Interfaces* 8 (2016) 9849–9854, <https://doi.org/10.1021/acsmami.6b00019>.

[35] R.G. Haverkamp, A.T. Marshall, B.C.C. Cowie, Energy resolved XPS depth profile of $(\text{IrO}_2, \text{RuO}_2, \text{Sb}_2\text{O}_5, \text{SnO}_2)$ electrocatalyst powder to reveal core-shell nanoparticle structure, *Surf. Interface Anal.* 43 (2011) 847–855, <https://doi.org/10.1002/sia.3644>.

[36] Z.P. Wang, J.H. Huang, L. Wang, Y.Y. Liu, W.H. Liu, S.L. Zhao, Z.Q. Liu, Cation-Tuning Induced d-Band Center Modulation on Co-Based Spinel Oxide for Oxygen Reduction/Evolution Reaction, e202114696, *Angew. Chem. Int. Ed.* 61 (2022), <https://doi.org/10.1002/ange.202114696>.

[37] Q.N. Song, M. Li, L.L. Wang, X.J. Ma, F. Liu, X. Liu, Mechanism and optimization of electrochemical system for simultaneous removal of nitrate and ammonia, *J. Hazard. Mater.* 363 (2019) 119–126, <https://doi.org/10.1016/j.jhazmat.2018.09.046>.

[38] L. Tian, M. Zhu, L.S. Zhang, L.J. Zhou, J.P. Fan, D.S. Wu, J.P. Zou, New insights on the role of NaCl electrolyte for degradation of organic pollutants in the system of electrocatalysis coupled with advanced oxidation processes, *J. Environ. Chem. Eng.* 10 (2022), 107414, <https://doi.org/10.1016/j.jece.2022.107414>.

[39] L. Tian, P. Chen, X.H. Jiang, L.S. Chen, L.L. Tong, H.Y. Yang, J.P. Fan, D.S. Wu, J. P. Zou, S.L. Luo, Mineralization of cyanides via a novel Electro-Fenton system generating $\cdot\text{OH}$ and $\cdot\text{O}_2$, *Water Res* 209 (2022), 117890 <https://doi.org/10.1016/j.watres.2021.117890>.

[40] Y. Yang, Recent advances in the electrochemical oxidation water treatment: spotlight on byproduct control, *Front Environ. Sci. Eng.* 14 (2020) 1–12, <https://doi.org/10.1007/s11783-020-1264-7>.

[41] L. Tian, L.S. Zhang, L.L. Zheng, Y. Chen, L. Ding, J.P. Fan, D.S. Wu, J.P. Zou, S. L. Luo, Overcoming electrostatic interaction via strong complexation for highly selective reduction of CN[–] into N₂, e202214145, *Angew. Chem. Int. Ed.* 61 (2022), <https://doi.org/10.1002/anie.202214145>.

[42] L. Tian, M.Y. Yin, L.L. Zheng, Y. Chen, W. Liu, J.P. Fan, D.S. Wu, J.P. Zou, S.L. Luo, Extremely efficient mineralizing CN[–] into N₂ via a newly developed system of generating sufficient $\text{ClO}^{\bullet}/\text{Cl}_2^{\bullet}$ and self-decreasing pH, *Sep. Purif. Technol.* 309 (2023), 123021, <https://doi.org/10.1016/j.seppur.2022.123021>.

[43] L.S. Zhang, X.H. Jiang, Z.A. Zhong, L. Tian, Q. Sun, Y.T. Cui, X. Lu, J.P. Zou, S. L. Luo, Carbon nitride supported high-loading fe single-atom catalyst for activation of peroxymonosulfate to generate $\cdot\text{O}_2$ with 100% selectivity, *Angew. Chem. Int. Ed.* 60 (2021) 21751–21755, <https://doi.org/10.1002/anie.202109488>.

[44] C.H. Zhou, J.H. Li, Y. Zhang, J. Bai, L. Li, X.J. Mei, X.H. Guan, B.X. Zhou, Novel denitrification fuel cell for energy recovery of nitrate-N and TN removal based on NH₄⁺ generation on a CNW@CF cathode, *Environ. Sci. Technol.* 56 (2022) 2562–2571, <https://doi.org/10.1021/acs.est.1c04363>.

[45] Y. Zhang, Y.Z. Ji, J.H. Li, J. Bai, S. Chen, L.S. Li, J.C. Wang, T.S. Zhou, P.Y. Jiang, X. H. Guan, B.X. Zhou, Efficient ammonia removal and toxic chlorate control by using BiVO₄/WO₃ heterojunction photoanode in a self-driven PEC-chlorine system, *J. Hazard. Mater.* 402 (2021), 123725, <https://doi.org/10.1016/j.jhazmat.2020.123725>.

[46] H.W. Lim, D.K. Cho, J.H. Park, S.G. Ji, Y.J. Ahn, J.Y. Kim, C.W. Lee, Rational design of dimensionally stable anodes for active chlorine generation, *ACS Catal.* 11 (2021) 12423–12432, <https://doi.org/10.1021/acscatal.1c03653>.

[47] J.J. Cai, H.J. Zhang, L.Z. Zhang, Y.Q. Xiong, T. Ouyang, Z.Q. Liu, Hetero-anionic structure activated Co–S bonds promote oxygen electrocatalytic activity for high-efficiency zinc–air batteries, *Adv. Mater.* (2023) 2303488, <https://doi.org/10.1002/adma.202303488>.

[48] C.L. Song, Q. Zhan, F. Liu, C. Wang, H.C. Li, X. Wang, X.F. Guo, Y.C. Cheng, W. Sun, L. Wang, J.S. Qian, B.C. Pan, Overturning loading of inert CeO₂ to active Co_3O_4 for unusually improved catalytic activity in fenton-like reactions, *Angew. Chem. Int. Ed.* 61 (2022), e20220406, <https://doi.org/10.1002/anie.20220406>.

[49] Y. Zhang, J.H. Li, J. Bai, L.S. Li, S. Chen, T.S. Zhou, J.C. Wang, L.G. Xia, Q.J. Xu, B. X. Zhou, Extremely efficient decomposition of ammonia N to N₂ using ClO^{\bullet} from reactions of HO[•] and HOCl generated *in Situ* on a novel bifacial photoelectrode, *Environ. Sci. Technol.* 53 (2019) 6945–6953, <https://doi.org/10.1021/acs.est.9b00959>.